

Duality-mediated critical amplitude ratios for the $(2 + 1)$ -dimensional $S = 1$ XY model

Yoshihiro Nishiyama

Department of Physics, Faculty of Science, Okayama University, Okayama 700-8530, Japan

Received: date / Revised version: date

Abstract. The phase transition for the $(2 + 1)$ -dimensional spin- $S = 1$ XY model was investigated numerically. Because of the boson-vortex duality, the spin stiffness ρ_s in the ordered phase and the vortex-condensate stiffness ρ_v in the disordered phase should have a close relationship. We employed the exact diagonalization method, which yields the excitation gap directly. As a result, we estimate the amplitude ratios $\rho_{s,v}/\Delta$ (Δ : Mott insulator gap) by means of the scaling analyses for the finite-size cluster with $N \leq 22$ spins. The ratio ρ_s/ρ_v admits a quantitative measure of deviation from selfduality.

PACS. 75.10.Jm Quantized spin models – 05.70.Jk Critical point phenomena – 75.40.Mg Numerical simulation studies – 05.50.+q Lattice theory and statistics (Ising, Potts, etc.)

1 Introduction

The $(2+1)$ -dimensional boson system undergoes the superfluid-insulator transition, which belongs to the three-dimensional XY universality class. The system possesses the boson-vortex duality [1, 2, 3], which brings about rich characters as to the critical phenomenon. The superfluid (ordered) and insulator (disordered) phases are characterized by the spin- and vortex-condensate-stiffness constants $\rho_{s,v}$, respectively. The critical amplitude ratio ρ_s/ρ_v admits a

“quantitative measure” [4] of deviation from selfduality.

Note that each stiffness constant $\rho_{s,v}$ yields the Drude weight for the corresponding AC conductivity [5], and it may be accessible [4] experimentally [6, 7, 8]. In this sense, the duality-mediated amplitude ratio is not a mere theoretical concept.

In Fig. 1, we present a schematic drawing for the stiffness constants (order parameters) $\rho_{s,v}$, which develop in the superfluid ($\delta J_{NN} > 0$) and insulator ($\delta J_{NN} < 0$) phases, respectively. In the respective phases, there open

Send offprint requests to:

the Higgs-mass m_H and the Mott-insulator Δ gaps above the ground state; in the terminology of the quantum spin model, the former (latter) corresponds to the longitudinal mode of the magnetic moment (paramagnetic massive excitation). (On the one hand, the Goldstone excitation corresponds to the transverse mode of the magnetic moment.) A key ingredient is that these quantities possess the identical scaling dimension, and the amplitude ratios among them make sense.

Recently, the duality-mediated amplitude ratios $\rho_{s,v}/\Delta$ came under theoretical investigation by means of the Monte Carlo [4, 9] and renormalization-group [10, 11, 12] methods. In prior to these studies, the mass-gap amplitude ratio m_H/Δ has been investigated rather extensively [9, 13, 14, 15, 16, 17]. As a matter of fact, for the two-dimensional ultra cold atom, these mass gaps were observed in proximity to the superfluid-insulator transition [18]; see Ref. [19] for a review.

The aim of this paper is to investigate these amplitude ratios for the $(2 + 1)$ -dimensional $S = 1$ XY model (1) by means of the exact diagonalization method. This method allows us to calculate the energy gaps such as m_H and Δ without resorting to the inverse Laplace transformation [9]. Moreover, the ground-state resolvent (response function) such as the second term of Eq. (5) is evaluated by means of the continued-fraction-expansion method [20]; the continued-fraction-expansion method is essentially the same as the Lanczos tri-diagonalization algorithm, and computationally less demanding. Otherwise, the finite-temperature effect (anisotropy between the imaginary

time and real-space system sizes) has to be considered carefully [21].

The Hamiltonian for the two-dimensional $S = 1$ XY model is given by

$$\mathcal{H} = -J_{NN} \sum_{\langle ij \rangle} (S_i^x S_j^x + S_i^y S_j^y) - J_{NNN} \sum_{\langle\langle ij \rangle\rangle} (S_i^x S_j^x + S_i^y S_j^y) + D_{\square} \sum_{[ijkl]} (S_i^z + S_j^z + S_k^z + S_l^z)^2 + D \sum_{i=1}^N (S_i^z)^2, \quad (1)$$

with the $S = 1$ -spin operators $\{\mathbf{S}_i\}$ placed at the square-lattice points, $i = 1, 2, \dots, N$. Here, the summations $\sum_{\langle ij \rangle}, \sum_{\langle\langle ij \rangle\rangle}, \sum_{[ijkl]}$ run over all possible nearest-neighbor $\langle ij \rangle$, next-nearest-neighbor $\langle\langle ij \rangle\rangle$, and plaquette spins $[ijkl]$, respectively. The parameters $J_{NN, NNN}$ and D_{\square} are the corresponding coupling constants. The symbol D denotes the single-ion anisotropy. We restrict ourselves to the parameter subspace

$$(J_{NN}, J_{NNN}, D_{\square}, D) = (J_{NN}^*, J_{NNN}^*, D_{\square}^*, D^*) + (\delta J_{NN}, \delta J_{NNN}, \delta D_{\square}, 0), \quad (2)$$

beside the critical point [22]

$$(J_{NN}^*, J_{NNN}^*, D_{\square}^*, D^*) = (0.158242810160, 0.058561393564, 0.10035104389, 0.9573),$$

The critical point (3) was fixed [22] so as to suppress corrections to scaling; namely, the critical point was determined via a preliminary approximate real-space-decimation method followed by the (ordinary) finite-size-scaling scheme.

The rest of this paper is organized as follows. In the next section, we present the simulation results. A comparison with the preceding results is made as well. In Sec. 3, we address the summary and discussions.

2 Numerical results

In this section, we present the numerical results. We employed the exact diagonalization method for the two-dimensional $S = 1$ XY model (1). We implemented the screw-boundary condition [23], which enables us to treat a variety of system sizes $N = 10, 12, \dots, 22$; the simulation algorithm is presented in Ref. [22]. Because the N spins constitute a rectangular cluster, the linear dimension of the cluster is given by $L = \sqrt{N}$, which sets a fundamental length scale for the scaling analyses.

2.1 Scaling behavior of the spin stiffness ρ_s : Analysis of ρ_s/m_H

In this section, we investigate the scaling behavior for the spin stiffness (superfluid density) ρ_s (5). We look into the interaction subspace

$$(\delta J_{NN}, \delta J_{NNN}, \delta D_{\square}) = \left(\delta J_{NN}, \frac{J_{NNN}^* \delta J_{NN}}{J_{NN}^*}, 0 \right), \quad (4)$$

parameterized by δJ_{NN} . In a preliminary survey, we found that within this interaction subspace, the ratio ρ_s/m_H is kept invariant for a considerably wide range of δJ_{NN} .

In Fig. 2, we present the scaling plot, $\delta J_{NN} L^{1/\nu} - L \rho_s(\delta J_{NN})$, for various (+) $N = 18$, (\times) 20 , and (*) 22 . Here, the scaling parameter ν is set to $\nu = 0.6717$, which is taken from the existing literatures, Ref. [24, 25]; note that the superfluid-insulator criticality belongs to the three-dimensional XY universality class. Hence, there is no adjustable fitting parameter involved in the present scaling analysis.

The spin stiffness is given by the formula

$$\rho_s = \frac{1}{N} \langle 0 | T | 0 \rangle + \frac{2}{N} \left\langle 0 \left| J \frac{\mathcal{P}}{\mathcal{H} - E_0} J \right| 0 \right\rangle, \quad (5)$$

with the ground-state energy (vector) E_0 ($|0\rangle$), projection operator $\mathcal{P} = 1 - |0\rangle\langle 0|$, the current operator J , and the diamagnetic contribution T ; explicit expressions for J and T are presented in Appendix. We stress that the *ground state* resolvent (the second term of Eq. (5)) is readily evaluated with the continued-fraction expansion [20].

The data in Fig. 2 appear to collapse into a scaling function satisfactorily, indicating that the simulation result reaches the scaling regime. As mentioned in Introduction, corrections to scaling are suppressed by finely adjusting [22] the interaction parameters to Eq. (3). As shown in Fig. 1. The spin stiffness ρ_s increases (decreases) in the superfluid (insulator) phase; see Fig. 1 as well. The scaling plot in Fig. 2 indicates that the ordinate $L\rho_s$ is dimensionless. That is, the stiffness constant possesses the scaling dimension of either reciprocal correlation length or excitation gap. Therefore, it is expected that the ratio ρ_s/m_H should be a universal constant.

Stimulated by this observation, we turn to the analysis of the amplitude ratio ρ_s/m_H . In Fig. 3, we present the scaling plot, $\delta J_{NN} L^{1/\nu} - \rho_s(\delta J_{NN})/m_H(\delta J_{NN})$, for (+) $N = 18$, (\times) 20 , and (*) 22 ; the scaling parameter ν is the same as that of Fig. 2. The Higgs mass m_H is evaluated by the formula $m_H = E_1 - E_0$ with the first-excitation energy E_1 specified by the the zero-momentum ($k = 0$) and zero-total-magnetization ($S^z = 0$) indices; the Goldstone mode belongs to the Hilbert-space sector with $S^z = \pm 1$ and $k = 0$. (In this way, we are able to estimate the excitation gaps in a straightforward manner without resorting to the inverse Laplace transformation [9].) A plateau ex-

tends around $\delta J_{NN} L^{1/\nu} > 0.5$. Such a feature indicates that the amplitude ratio ρ_s/m_H takes a constant value in proximity to the critical point.

In Fig. 4, we plot the approximate amplitude ratio ρ_s/m_H for $1/L^2$. Here, the approximate amplitude ratio ρ_s/m_H denotes the plateau height

$$\left. \frac{\rho_s(\delta J_{NN})}{m_H(\delta J_{NN})} \right|_{\delta J_{NN}=\delta \bar{J}_{NN}}, \quad (6)$$

at the extremal point, $\partial_{\delta J_{NN}}(\rho_s/m_H)|_{\delta J_{NN}=\delta \bar{J}_{NN}} = 0$, for each system size $N(=L^2) = 10, 12, \dots, 22$. The least-squares fit to these data yields an estimate $\rho_s/m_H = 0.1627(23)$ in the thermodynamic limit $L \rightarrow \infty$. In order to appreciate a possible systematic error, we make an alternative extrapolation. The irregularities (bumps) around $1/L^2 = 0.05 (\approx 1/4.5^2)$ and $0.08 (\approx 1/3.5^2)$ are due to the artifact of the screw-boundary condition [23]. In order to avoid these intermittent irregularities, we consider a sector $N = 14, 16, \dots, 20$, for which the least-squares fit leads to an estimate $\rho_s/m_H = 0.1551(25)$. The discrepancy ≈ 0.008 between the independent extrapolations may indicate a possible systematic error. Putting both least-squares-fit and systematic errors into consideration, we estimate the amplitude ratio as

$$\rho_s/m_H = 0.16(1). \quad (7)$$

A remark is in order. According to our preliminary survey, the combination ρ_s/m_H turned out to be an optimal one in the sense that the ratio exhibits a stable plateau for a considerably wide range of δJ_{NN} . Experimentally, the Higgs mass m_H became observable even in close vicinity of the critical point [18].

2.2 Scaling behavior of the vortex-condensate

stiffness ρ_v : Analysis of ρ_s/ρ_v

In this section, we analyze the amplitude ratio $\rho_s(\delta J_{NN})/\rho_v(-\delta J_{NN})$. For that purpose, we survey the parameter subspace

$$(\delta J_{NN}, \delta J_{NNN}, \delta D_{\square}) = \left(\delta J_{NN}, \frac{J_{NNN}^* \delta J_{NN}}{J_{NN}^*}, \frac{1.4 D_{\square}^* \delta J_{NN}}{J_{NN}^*} \right), \quad (8)$$

parameterized by a single variable δJ_{NN} . In a preliminary survey, we found that within this subspace, the amplitude ratio ρ_s/ρ_v exhibits a stable plateau in an appreciable range of δJ_{NN} .

In Fig. 5, we present the scaling plot, $\delta J_{NN} L^{1/\nu} - \rho_s(\delta J_{NN})/\rho_v(-\delta J_{NN})$ for (+) $N = 18$, (\times) 20 , and ($*$) 22 ; the scaling parameter ν is the same as that of Fig. 2. Here, the vortex-condensate stiffness ρ_v is given [4] by $\rho_v = (2\pi)^{-2} k_1^2 / \chi_{\rho}(k_1)$ with the charge-density-wave susceptibility $\chi_{\rho}(k)$ and $k_1 = 2\pi/N$; the explicit expression for χ_{ρ} is presented in Appendix. The plateau extending around $\delta J_{NN} L^{1/\nu} > 0.2$ indicates that the amplitude ratio ρ_s/ρ_v is indeed a universal constant.

In Fig. 6, we present the approximate ratio ρ_s/ρ_v for $1/L^2$. Here, the approximate ratio ρ_s/ρ_v denotes the plateau height

$$\left. \frac{\rho_s(\delta J_{NN})}{\rho_v(-\delta J_{NN})} \right|_{\delta J_{NN}=\delta \bar{J}_{NN}}, \quad (9)$$

with $\partial_{\delta J_{NN}}(\rho_s/\rho_v)|_{\delta J_{NN}=\delta \bar{J}_{NN}} = 0$ for each $N = 10, 12, \dots, 22$.

The least-squares fit to these data yields an estimate $\rho_s/\rho_v = 0.1731(50)$ in the thermodynamic limit $L \rightarrow \infty$. The irregularity around $1/L^2 = 0.05 (\approx 1/4.5^2)$ may be due to the artifact of the screw-boundary condition [23]. As in Sec. 2.1, we consider an intermediate sector $N = 14, 16, \dots, 20$,

for which the least-squares fit leads to an estimate $\rho_s/\rho_v = 0.1820(67)$. The discrepancy ≈ 0.009 between the independent extrapolations may provide an indicator for a possible systematic error. Putting both least-squares-fit and systematic errors into consideration, we estimate the amplitude ratio as

$$\rho_s/\rho_v = 0.17(2). \quad (10)$$

The amplitude ratio provides a “quantitative measure” [4] of deviation from selfduality; we stress that the formal duality argument does not fix the ratio ρ_s/ρ_v quantitatively.

2.3 Amplitude ratios $\rho_{s,v}/\Delta$

In this section, we dwell on the expressions, $\rho_{s,v}/\Delta$, which are the central concern in the preceding studies. A comparison with these studies follows. For that purpose, we resort to a relation $m_H/\Delta = 2.1(2)$ [15]. Based on this relation, we convert the results, Eqs. (7) and (10), into

$$\rho_s/\Delta = 0.34(4), \quad (11)$$

and

$$\rho_v/\Delta = 2.0(4). \quad (12)$$

This is a good position to address an overview of the related studies; see Table 1. According to the Monte Carlo simulation [9,4], the results, $\rho_s/\Delta = 0.44(1)$, $\rho_v/\Delta = 2.1(1)$ and $\rho_s/\rho_v = 0.21(1)$, were obtained. An elaborated non-perturbative-renormalization-group analysis [10] yields $\rho_s/\Delta = 0.414$, $\rho_v/\Delta = 1.98$ and $\rho_s/\rho_v = 0.210$. As a reference, we recollect pioneering renormalization-group results, $\rho_s/\Delta = 0.386$ [11] and $\rho_s/\Delta = 0.2642$ [12]. The large- N analysis arrives at $\rho_v/\Delta = \frac{12}{2\pi} = 1.909\dots$ [26].

As mentioned above, the results for ρ_s/Δ have not yet been settled. Our result $\rho_s/\Delta = 0.34(4)$, Eq. (11), seems to support the pioneering renormalization-group study [11]. That is, our result displays a tendency toward a suppression of ρ_s , as compared to the Monte Carlo result. As for the dual counterpart ρ_v/Δ , our result $\rho_v/\Delta = 2.0(4)$, Eq. (12), agrees with the above-mentioned preceding studies. It would be intriguing that the large- N result $\rho_v/\Delta = 1.909\dots$ [26] is approved by these elaborated analyses. As to ρ_s/ρ_v , our result $\rho_s/\rho_v = 0.17(2)$, Eq. (10), lies out of the above-mentioned results, again reflecting a tendency toward a suppression of ρ_s .

3 Summary and discussions

The duality-mediated critical amplitude ratios were investigated for the $(2 + 1)$ -dimensional $S = 1$ XY model (1). We employed the exact diagonalization method, which enables us to calculate the energy gap directly; as shown in Fig. 1, the energy gap provides a fundamental unit for the stiffness constants $\rho_{s,v}$. Based on the finite-size-scaling analyses, we obtained the estimates, $\rho_s/m_H = 0.16(1)$, Eq. (7), and $\rho_s/\rho_v = 0.17(2)$, Eq. (10). Thereby, we converted these results into $\rho_s/\Delta = 0.34(4)$, Eq. (11), and $\rho_v/\Delta = 2.0(4)$, Eq. (12) via $m_H/\Delta = 2.1(2)$ [15]. Our results are to be compared with the Monte Carlo estimates $(\rho_s/\Delta, \rho_v/\Delta, \rho_s/\rho_v) = (0.44(1), 2.1(1), 0.21(1))$ [9,4] and the renormalization-group ones, $(0.414, 1.98, 0.210)$ [10]. It has to be mentioned that the pioneering renormalization-group analyses arrived at $\rho_s/\Delta = 0.386$ [11] and $\rho_s/\Delta = 0.2642$ [12]. As for ρ_s/Δ , the results have not yet been set-

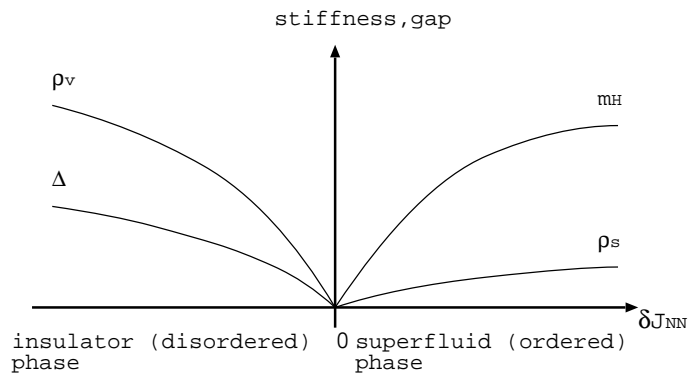


Fig. 1. The spin- and vortex-condensate-stiffness constants $\rho_{s,v}$ characterize the superfluid ($\delta J_{NN} > 0$) and insulator ($\delta J_{NN} < 0$) phases, respectively. Correspondingly, the Higgs-mass m_H and the Mott-insulator Δ gaps open above the ground state. These quantities have the same scaling dimension, and the critical amplitude ratios among them make sense. The ratio m_H/Δ has been investigated rather extensively so far [13, 14, 15, 16, 17].

tled. Our result displays a tendency toward a suppression of ρ_s , suggesting pronounced deviation from the naive self-duality relation $\rho_s/\rho_v = 1$. On the one hand, as to the dual counterpart ρ_v/Δ , the results are almost settled. Notably enough, the large- N result $\rho_v/\Delta = \frac{12}{2\pi} = 1.909\dots$ is approved by the elaborated calculations. It would be intriguing to examine the validity of the N -dependent generic results [10] systematically through extending the internal symmetries to $N = 3, 4, \dots$

Acknowledgment

This work was supported by a Grant-in-Aid for Scientific Research (C) from Japan Society for the Promotion of Science (Grant No. 25400402).

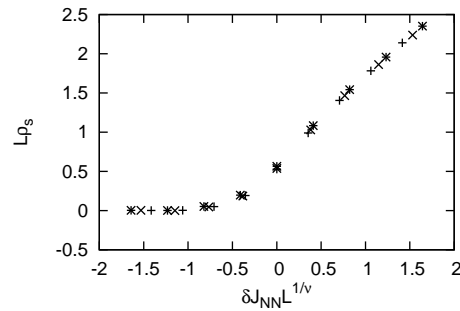


Fig. 2. The scaling plot, $\delta J_{NN} L^{1/\nu} - L\rho_s$, is presented for various system sizes (+) $N = 18$, (\times) 20 , and ($*$) 22 . Here, the scaling parameter $\nu = 0.6717$ is taken from the existing literatures [24, 25]; namely, there is no adjustable parameter involved in the scaling analysis. The spin stiffness ρ_s develops in the superfluid phase, $\delta J_{NN} > 0$.

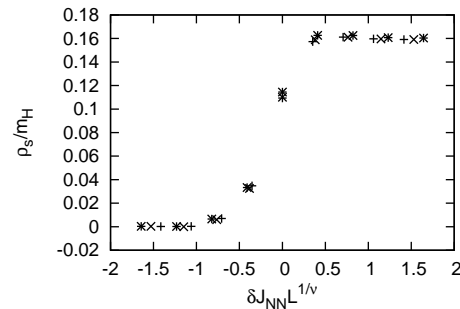


Fig. 3. The scaling plot, $\delta J_{NN} L^{1/\nu} - \rho_s(\delta J_{NN})/m_H(\delta J_{NN})$, is presented for various system sizes (+) $N = 18$, (\times) 20 , ($*$) 22 ; the scaling parameter ν is the same as that of Fig. 2. A plateau extends around $\delta J_{NN} L^{1/\nu} > 0.5$, suggesting that the amplitude ratio ρ_s/m_H takes a constant value.

Simulation algorithm: Screw-boundary condition

We implemented the screw-boundary condition [23] for the two-dimensional XY model (1). In short, an alignment of spins $\{\mathbf{S}_i\}$ ($i = 1, 2, \dots, N$) is arranged so as to form a toroidal-coil structure, which is equivalent to the

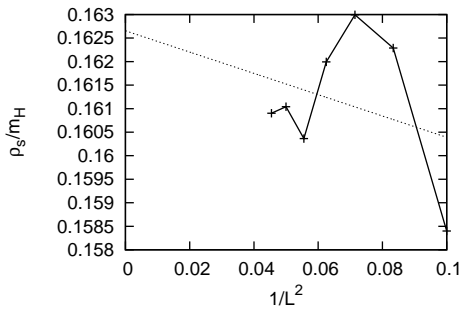


Fig. 4. The approximate amplitude ratio ρ_s/m_H (6) is plotted for $1/L^2$. The least-squares fit to these data yields an estimate $\rho_s/m_H = 0.1627(23)$ in the thermodynamic limit. The irregularities (bumps) around $1/L^2 = 0.05 (\approx 1/4.5^2)$ and $0.08 (\approx 1/3.5^2)$ are due to the artifact of the screw-boundary condition [23]. A possible systematic error is considered in the text.

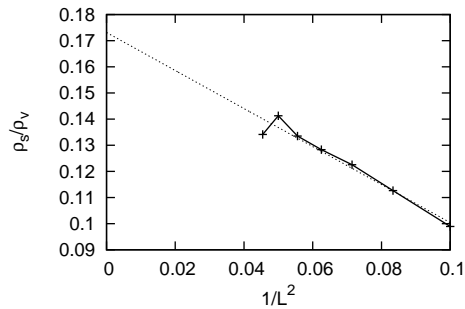


Fig. 6. The approximate amplitude ratio ρ_s/ρ_v (9) is plotted for $1/L^2$. The least-squares fit to these data yields an estimate $\rho_s/\rho_v = 0.1731(50)$ in the thermodynamic limit. The irregularity around $1/L^2 = 0.051 (\approx 1/4.5^2)$ is an artifact due to the screw-boundary condition [23]. A possible systematic error is considered in the text.

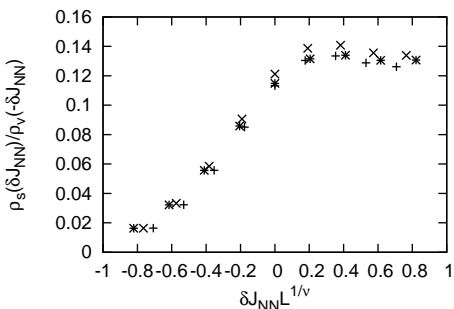


Fig. 5. The scaling plot, $\delta J_{NN} L^{1/\nu} - \rho_s(\delta J_{NN})/\rho_v(-\delta J_{NN})$, is presented for various system sizes (+) $N = 18$, (\times) 20, and ($*$) 22; the scaling parameter ν is the same as that of Fig. 2. A plateau extends around $\delta J_{NN} L^{1/\nu} > 0.2$, suggesting that the amplitude ratio ρ_s/ρ_v takes a universal constant.

two-dimensional cluster under the screw-boundary condition. We adopted the simulation algorithm presented in Ref. [22]. Here, for the sake of self-consistency, we present explicit expressions for the perturbation operators, J , T , and N_k in the screw-boundary-condition representation.

Table 1. A summary of the related studies is presented. The non-perturbative renormalization group (NPRG) has a number of variants. The abbreviations, DE and BMW, denote derivative expansion and Blaizot Méndez-Galain Wschebor, respectively.

Amplitude ratios	ρ_s/Δ	ρ_v/Δ	ρ_s/ρ_v
This work	0.34(4)	2.0(4)	0.17(2)
Monte Carlo [9,4]	0.44(1)	2.1(1)	0.21(1)
NPRG-DE [10]	0.414	1.98	0.210
NPRG-BMW [11]	0.386		
NPRG-DE [12]	0.2642		

The current operator J is given by

$$\begin{aligned}
 J = & \frac{iJ_{NN}}{2} \sum_{j=1}^N (S_j^+ S_j^-(1) - S_j^- S_j^+(1)) \\
 & + \frac{iJ_{NNN}}{2} \sum_{j=1}^N (S_j^+ S_j^-(\sqrt{N}+1) - S_j^- S_j^+(\sqrt{N}+1)) \\
 & - \frac{iJ_{NNN}}{2} \sum_{j=1}^N (S_j^+ S_j^-(\sqrt{N}-1) - S_j^- S_j^+(\sqrt{N}-1))
 \end{aligned}$$

with the δ -th-neighbor spin operator $S_j^\pm(\delta) = P^\delta S_j^\pm P^{-\delta}$, and the translation operator P ($P|\{S_i^z\}\rangle = |\{S_{i+1}^z\}\rangle$) [23].

The diamagnetic contribution T is given by

$$T = \frac{J_{NN}}{2} \sum_{j=1}^N (S_j^+ S_j^-(1) + S_j^- S_j^+(1)) \\ + \frac{J_{NNN}}{2} \sum_{j=1}^N (S_j^+ S_j^-(\sqrt{N} + 1) + S_j^- S_j^+(\sqrt{N} + 1)) \\ + \frac{J_{NNN}}{2} \sum_{j=1}^N (S_j^+ S_j^-(\sqrt{N} - 1) + S_j^- S_j^+(\sqrt{N} - 1)) \quad (14)$$

Similarly, the charge-density-wave operator is defined as $N_k = \sum_{j=1}^N e^{ikj} S_j^z$, and the charge-density-wave susceptibility is given by the formula $\chi_\rho(k) = \frac{1}{N} \langle 0 | N_k^\dagger (\mathcal{H} - E_0)^{-1} N_k | 0 \rangle$.

References

1. M. Stone and P. R. Thomas, Phys. Rev. Lett. **41**, 351 (1978).
2. M. P. A. Fisher and D. H. Lee, Phys. Rev. B **39**, 2756 (1989).
3. X. G. Wen and A. Zee, Int. J. Mod. Phys. B **04**, 437 (1990).
4. S. Gazit, D. Podolsky and A. Auerbach, Phys. Rev. Lett. **113**, 240601 (2014).
5. M. Swanson, Y. L. Loh, M. Randeria and N. Trivedi, Phys. Rev. X **4**, 021007 (2014).
6. J. Corson, R. Mallozz, J. Orenstein, J. N. Eckstein and I. Bozovic, Nature **398**, 221 (1999).
7. R. W. Crane, N. P. Armitage, A. Johansson, G. Sambandamurthy, D. Shahar and G. Grüner, Phys. Rev. B **75**, 094506 (2007).
8. J. F. Sherson, C. Eeitenberg, M. Endres, M. Cheneau, I. Bloch and S. Kuhr, Nature **467**, 68 (2010).
9. S. Gazit, D. Podolsky, A. Auerbach and D. P. Arovas, Phys. Rev. B **88**, 235108 (2013).
10. F. Rose and N. Dupuis, Phys. Rev. B **95**, 014513 (2017).
11. F. Rose, F. Léonard and N. Dupuis, Phys. Rev. B **91**, 224501 (2015).
12. A. Rançon, O. Kodio, N. Dupuis and P. Lecheminant, Phys. Rev. E **88**, 012113 (2013).
13. S. Gazit, D. Podolsky, and A. Auerbach, Phys. Rev. Lett. **110**, 140401 (2013).
14. K. Chen, L. Liu, Y. Deng, L. Pollet, and N. Prokof'ev, Phys. Rev. Lett. **110**, 170403 (2013).
15. Y. Nishiyama, Nucl. Phys. B **897**, 555 (2015).
16. A. Rançon and N. Dupuis, Phys. Rev. B **89**, 180501 (2014).
17. Y. T. Katan and D. Podolsky, Phys. Rev. B **91**, 075132 (2015).
18. M. Endres, T. Fukuhara, D. Pekker, M. Cheneau, P. Schauß, C. Gross, E. Demler, S. Kuhrand and I. Bloch, Nature **487**, 454 (2012).
19. D. Pekker and C.M. Varma, Annual Rev. Condens. Matter Phys. **6**, 269 (2015).
20. E. R. Gagliano and C. A. Balseiro, Phys. Rev. Lett. **59**, 2999 (1987).
21. See Supplemental Material of Ref. [4].
22. Y. Nishiyama, Phys. Rev. E **78**, 021135 (2008).
23. M. A. Novotny, J. Appl. Phys. **67**, 5448 (1990).
24. M. Campostrini, M. Hasenbusch, A. Pelissetto, and E. Vicari, Phys. Rev. B **74**, 144506 (2006).
25. E. Burovski, J. Machta, N. Prokof'ev, and B. Svistunov, Phys. Rev. B **74**, 132502 (2006).
26. K. Damle and S. Sachdev, Phys. Rev. B **56**, 8714 (1997).